J Mater Sci: Mater Electron (2020) 31:20578–20588

Characterization of the CoFe2O4/Cu displacement effect in the Y123 superconductor matrix on critical properties

S. Safran[1,*], F. Bulut[2], A. R. A. Nefrow[3], H. Ada[4], and O. Ozturk[3]

[1] Department of Physics, Ankara University, 06100 Ankara, Turkey
[2] Sinop University, Scientific and Technological Research Applications and Research Center, 57000 Sinop, Turkey
[3] Department of Electrical and Electronics Engineering, Kastamonu University, 37100 Kastamonu, Turkey
[4] Department of Mechanical Engineering, Kastamonu University, 37100 Kastamonu, Turkey

Received: 6 July 2020
Accepted: 30 September 2020
Published online: 8 October 2020

ABSTRACT

In this study, $CoFe_2O_4$ (x = 0, 5, 10 and 20 wt%) doped $YBa_2Cu_{3-x}(CoFe_2O_4)_xO_{7-\delta}$ bulk samples were produced using solid state reaction (SSR) method and sol–gel(SG) methods. Oxide-form and acetate-form powders were preferred for SSR method and SG method, respectively. The heat treatment of the produced samples was carried out in two stages. Firstly, the samples were annealed at 950 °C for 24 h, after which they were kept in oxygen at 500 °C for 5 h and allowed to be cooled down to room temperature. Characterization of all samples was performed using methods such as X-ray diffraction, scanning electron microscopy, energy dispersive spectroscopy, temperature-dependent resistance measurement (R–T) and Vickers microhardness analysis. Superconducting behavior was observed in all the produced samples, but as a result of the addition, a decrease was observed with the increase of the doping ratio at the critical transition temperature. As a result of the characterization, it is concluded that the doping ions can be replaced with Cu atoms in Y123 structure. In addition, doping led to significant changes in Vickers microhardness results.

1 Introduction

One of the most important advantages of $YBa_2Cu_3O_{7-\delta}$ (Y123) superconductor structure is that it has a transition temperature above the liquid nitrogen temperature as in other high temperature superconductors (HTS). In this way, superconductors can be used in many technological areas related to motors, transformers, material engineering, heavy industry technology and industrial energy etc. To use superconductors in technological applications, structural, electrical, magnetic and mechanical performance of materials are very crucial. In this context, different studies have been conducted to examine and improve the production methods and properties of YBCO, which has one of the copper-layer

Address correspondence to E-mail: safranserap@gmail.com

https://doi.org/10.1007/s10854-020-04578-y

superconductors [1–5]. Different methods of production [6–9], displacement [10, 11] or adding to the structure at certain stoichiometric rate [12, 13] were applied and the properties of the samples produced were investigated.

The SSR method is one of the most common methods in the production of polycrystalline YBCO superconductors. This method involves mixing of the powdered chemicals in stoichiometric proportions and annealing the mixture at high temperatures and at certain times. This method, where multiple grinding processes are applied to homogeneously mix the samples, is simple and frequently used. Non-reactive metal oxides or carbonate based components are often preferred as precursor materials [14–16]. In the SG method; achieving chemical homogeneity, ease of controlling particle size and its morphology have made this method a preferable method compared to solid state reaction method [14–17]. This wet chemical process is carried out by dissolving one or more metal components in solution [18].

In the study of Slimani et al. [19] in 2014, the effect of $CoFe_2O_4$ addition on phases of Y123 and Y358 was investigated. The samples produced by SSR method were shown to have single phase perovskite orthorhombic structure and the changes in the parameters of crystal lattice were evaluated. In this study, it has been concluded that the increase in $CoFe_2O_4$ additive decreases the critical temperature value and this situation is valid for both phases. While Y123 structure shows superconducting properties with 2 wt.% $CoFe_2O_4$ addition, another result achieved in this study is that the structure of Y358 does not show superconductivity of the same amount of additive sample. Similar results are observed in other studies examining the $CoFe_2O_4$ addition [20, 21]. The effect of $CoFe_2O_4$ addition on the Y123 and Y358 phases was studied as structural and electrical.

The main goal of the study is to analyze the effect of $CoFe_2O_4$ doping on structural, electrical, superconducting, and mechanical properties of Y123 bulk samples produced by SSR and SG methods. The effect of $CoFe_2O_4$ addition on YBCO produced by SSR method was investigated [19–21]. However, no studies have been conducted on $CoFe_2O_4$ doping on the mechanical properties of Y123 samples and also any study related to $CoFe_2O_4$ (x = 0, 5, 10 and 20 wt.%) doped $YBa_{2-x}Cu_3O_{7-\delta}$ prepared by SG method has not been addressed.

2 Experimental

In this study, two different methods were used for the preparation of $CoFe_2O_4$ doping Y123 superconducting samples. $CoFe_2O_4$ (nanopowder, 30 nm particle size (TEM), 99%, Sigma-Aldrich) was used as doping material for the samples produced by SSR method and SG methods. Y_2O_3 (99.99%, Alfa Aesar), $BaCO_3$ (99.95%, Alfa Aesar) and CuO (99.9995%, Alfa Aesar) precursor powders were preferred to produce samples by SSR method. In the SG method, 15 mL of acetic acid and 15 mL of anhydrous methanol were added to the barium acetate powder (99.999% trace metals basis, Sigma-Aldrich) and mixed at room temperature until a homogeneous mixture of barium was obtained. The resulting solution was added to yttrium acetate powder (99.9% metals basis, Sigma-Aldrich) and mixed once more. After homogeneity was achieved, the doping element and copper acetate were added up the mixture with adding 8 mL of triethanolamine (≥ 99.0, Sigma-Aldrich). Triethanolamine is used for accelerating the dissolution process of copper. The obtained turquoise homogeneous solution could stir in a sealed beaker at room temperature for 12 h, and then the beaker was opened and heated to 80 °C for gelling of the solution. The solution, which reached the consistency of gel, was applied to heat treatment in the oven at 300 °C for 30 min.

In this study, starting powders were weighed considering 1:2:3 stoichiometric ratios for sample production in the determined phase. The doping ratio for the structure of $YBa_2Cu_{3-x}(CoFe_2O_4)_xO_{7-\delta}$ was made by weight at $0 \leq x \leq 0.20$. The stoichiometrically weighed starting powders were initially milled in an agate mortar for 1 h. The powder mixture was placed in alumina boats and calcined at 850 °C for 24 h in furnace three times. $CoFe_2O_4$ was added into mixed powders at 0 wt.%, 5 wt.%, 10 wt.% and 20 wt.%. The powders were pressed into pellets 10 mm in diameter and 2 mm in thickness under 200 MPa pressure using a hydraulic press. The samples were annealed in air at 930 °C for 24 h and then lowered to 500 °C and subjected to oxygen for 5 h. The samples are called as SSR-0, SSR-5, SSR-10, SSR-20 and SG-0, SG-5, SG-10 and SG-20. SSR and SG mean solid state reaction method and sol–gel method, respectively. The numbers following SSR and SG represent the addition ratio in wt.%.

XRD measurements were carried out by Bruker D8 Advance diffractometer with CuK_α ($\lambda = 1.541$Å) radiation between $2\theta = 3°$–$90°$ for scanning speed of 4°/min. SEM images were taken by JEOL JSM-5300 with × 2500 and × 10,000 magnitude and EDS analysis was obtained from SEM measurements for the surface morphology. The electrical resistivity was measured in Janis CCS-450 by conventional four-probe method for the temperature range of 10–300 K. SHIMADZU HVM-2 microhardness tester was used for microhardness test and measurements were performed at room temperature.

3 Results and discussion

3.1 Structural analysis

3.1.1 XRD analysis

XRD patterns of undoped and $CoFe_2O$ doped samples produced by SSR and SG method are shown in Fig. 1a and b, respectively. The diffraction line intensities are decreasing, and they are shifting to low angles with increasing doping ratio produced in both methods. In this case, it may conclude that doping affects the crystallinity of the material. XRD patterns also show that there are no impurity peaks associated with Co and Fe atoms. It can be said that Cu^{+2} ions may have partly replaced by Co^{+3} and Fe^{+2} ions, the electron density in the structure will increase and superconductivity will be negatively affected. It is seen from Fig. 1 that doped and undoped Y-123 superconducting materials crystallize in the orthorhombic symmetry independent of the preparation method. The a, b and c lattice parameters obtained from XRD data were calculated for orthorhombic structure using the following formula given by;

$$\frac{1}{d^2} = \frac{h^2}{a^2} + \frac{k^2}{b^2} + \frac{l^2}{c^2} \quad (1)$$

and the crystallite size of the samples

$$D = \frac{0.941\lambda}{B\cos\theta} \quad (2)$$

$$B^2 = B_s^2 - B_m^2 \quad (3)$$

was also calculated using Eqs. (2) and (3). Here θ and B_s represent Bragg angle, the full width half maximum (FWHM) value for the (103) diffraction line,

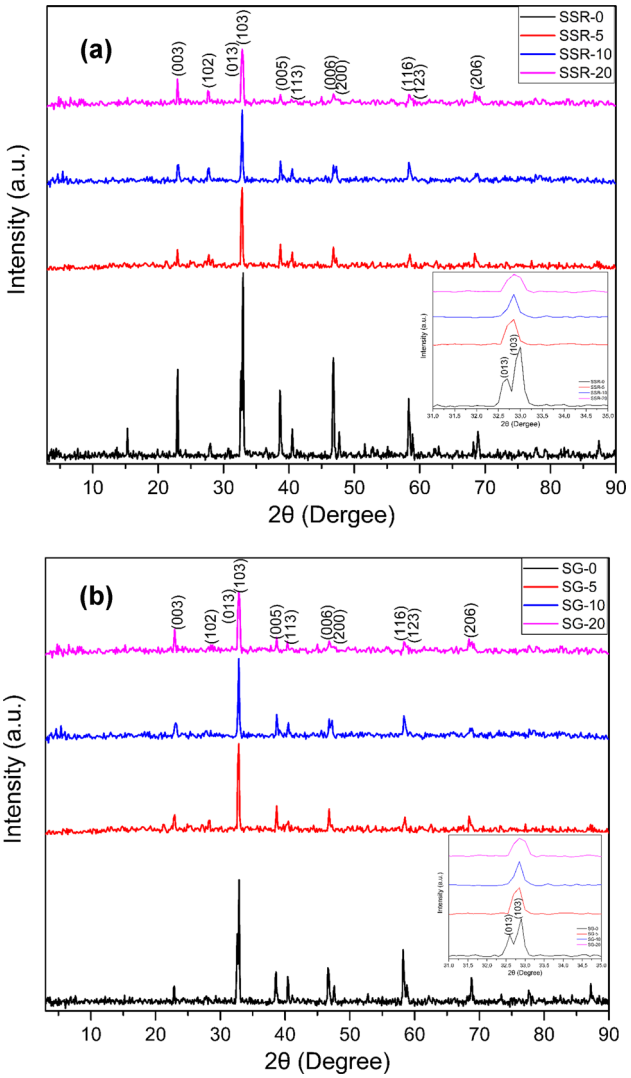

Fig. 1 XRD graph and miller indices of samples produced by **a** solid state reaction, **b** sol–gel methods

respectively and $B_m = 0.000007$. B_s value considerably vary, depending on the crystallite size geometry and distribution. D are only estimated values calculated using the FWHM of diffraction lines. The calculated grain sizes, lattice parameters and orthorhombicity value ($\delta = 100(a-b)/(a+b)$), reduction in diffraction line intensities and the shifting of peaks to low angles are consistent with the orthorhombicity values given in Table 1. A significant decrease on b lattice parameter of the materials depending increase on doping can also explain the decrement of orthorhombicity value. The inset of Fig. 1 shows (013) and (103) diffraction lines which give information about orthorhombicity of YBCO structure. In the orthorhombic structure of the YBCO compound, the

intensity of the (013) peak is smaller than the intensity of the (103) peak and these peaks are very close to each other [22]. In the tetragonal structure of the YBCO compound, (013) and (103) peaks are overlapped. It is apparently seen that diffraction peaks of (013) and (103) merge with doping. From the inset of Fig. 1 and decreasing values of δ (Table 1) show that orthorhombic structure starts to convert tetragonal structure. This negatively affects superconducting properties. Critical temperature (T_c) values of SSR-20 and SG-20 which are the highest wt % doped samples are 50.94 K and 25.31 K, respectively, these values are far below the 90 K which is the T_c value of undoped sample. In the literature, the values of lattice parameters for the standard Y-123 phase are given as a = 3.82 Å, b = 3.88 Å and c = 11.69 Å [14, 15]. According to the values of lattice parameters given in Table 1, it is seen that the values of the samples produced for SSR method is in accordance with the literature. However, it is clear that the doping leads to changes in the lattice parameters for SG method. Doping process in samples produced by SSR method has caused changes in particle size values. Particle size values in samples except that SSR-20 slightly increased with rising doping ratio. Although the particle size increased with doping in the SSR method, highest wt % doped sample caused a decrease in the particle size. There is no systematic change in particle size in samples produced by SG method.

3.1.2 SEM and EDS analysis

The surface morphology, particle distributions, particle boundaries and particle sizes of the produced samples were examined by SEM images. Figures 2a–d and 3a–d illustrate the SEM images of SSR and SG samples, respectively. These images are taken with × 2500, the inset of figures illustrates × 10,000 magnification. For both methods, the porous structure of the doping samples and the changes on the surface of the adding process can be seen from the figure. However, it can be said that the samples produced by the SSR method have a more porous surface than the samples produced by the SG method. The samples contain randomly oriented and granular structures in both methods. We consider that $CoFe_2O$ can be able to re-arrange the YBCO crystal structure which includes elements (Y, Ba, Cu, O) due to the convenience of ionic radius. As given in Table 2, ionic radius of Fe^{2+} and Co^{3+} is comparable with ionic radius of Y^{3+} and Cu^{2+}. Substitution can be possible with convenient ionic radius. Cobalt and iron impurities entering the structure with the increase of the doping ratio cause a decrease in porosity in the structure and play a role in the change of particle boundaries. However, there is an optimal value of addition (5 wt.%), after this addition the surface morphology is adversely affected, and grain boundaries are deteriorated.

The elements in the structure and percent distributions of these elements by EDS analysis are given in Table 3 and EDS analysis of SSR-5 and SG-5 are shown in Fig. 4a and b, respectively. From the graphs and tables, it is seen that O and Ba ratios are almost constant and with increasing ratio of doping, however, the amount of Cu and Y decrease while Fe and Co increase by weight. Increasing the ratio of $CoFe_2O_4$ addition clarifies the broadening of superconducting transition interval (0 $T_C\left(T_C^{\text{onset}} - T_C^{\text{offset}}\right)$ (Table 4). Because Fe and Co ions enter the structure instead of Cu and Y ions with the addition. The difference electronegativity of Fe and Co to Cu and Y can be reason for this substitution (Electronegativity values of elements are given in Table 2). If Cu and Y substitutes for Fe and Co, electronegativity of the YBCO matrix is raised and this can be increased the

Table 1 Crystallite size and lattice cell parameters for all the $YBa_2Cu_{3-x}(CoFe_2O_4)_xO_{7-\delta}$ ceramic superconductors

Sample	Crystallite size (Å)	a (Å)	b (Å)	c (Å)	Volume (V)	Orthorhombicity (δ)
SSR-0	29	3.82	3.88	11.68	173.02	0.87
SSR-5	30	3.82	3.87	11.63	172.11	0.66
SSR-10	31	3.81	3.87	11.63	171.78	0.79
SSR-20	25	3.81	3.86	11.61	170.58	0.59
SG-0	28	3.82	3.90	11.62	173.10	0.98
SG-5	30	3.88	3.86	11.63	174.30	0.26
SG-10	29	3.87	3.84	11.62	172.88	0.40
SG-20	28	3.87	3.84	11.61	172.68	0.37

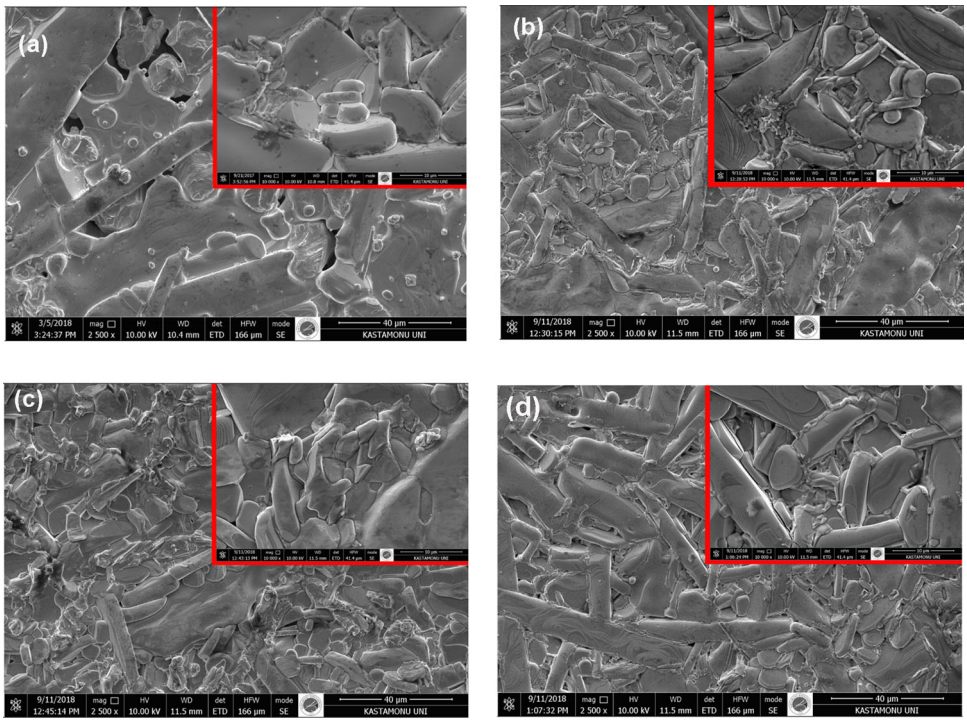

Fig. 2 SEM images for **a** SSR-0, **b** SSR-5, **c** SSR-10, **d** SSR-20 superconducting materials produced by solid state reaction method

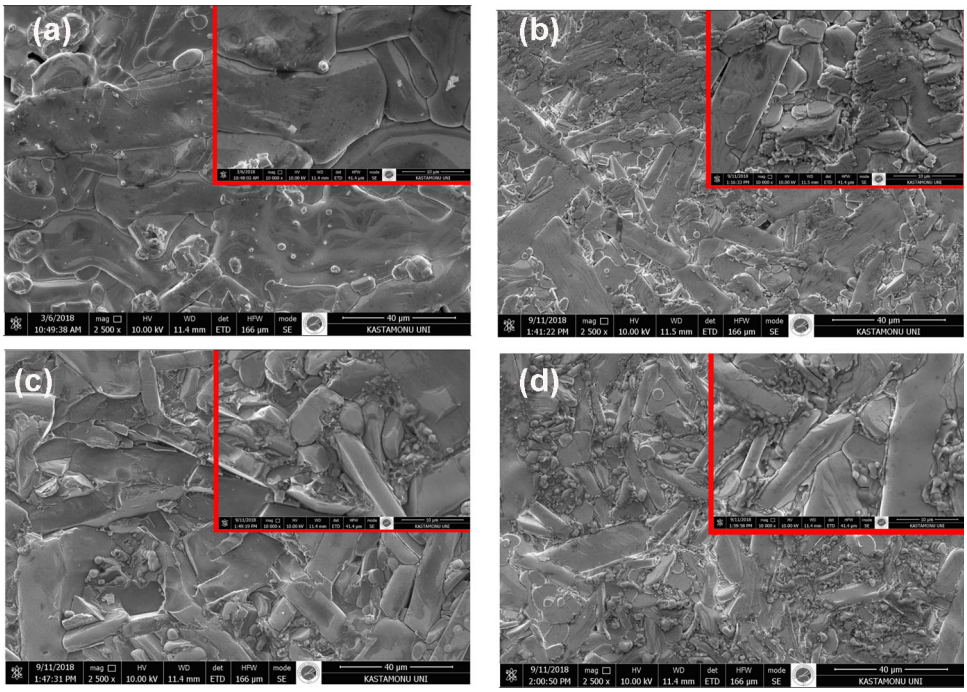

Fig. 3 SEM images for **a** SG-0, **b** SG-5, **c** SG-10, **d** SG-20 superconducting materials produced by sol–gel method

mobile hole density so CuO_2 planes is increased [23]. We can deduce from that some cobalt and iron atoms may partly be displaced properly by the copper and yttrium sites in the Y-123 crystal lattice. In addition, remaining $CoFe_2O_4$ atoms without displacement can accumulate at grain boundaries and causes weak links. This situation also supports the changings in superconductivity properties like T_C.

Table 2 Ionic radius and electronegativity values of elements used in this study

Atom No	Element	Ionic radius (pm)	Electronegativity
8	O^{2-}	73	3.4
39	Y^{3+}	90	1.2
56	Ba^{2+}	135	0.9
29	Cu^{2+}	77	1.9
26	Fe^{2+}	70	1.8
27	Co^{3+}	60	1.9

Table 3 Local percent distributions of elements measured by EDS

Sample name	Weight %					
	OK	YL	BaL	CuK	FeK	CoK
SSR-0	15.59	11.91	44.59	29.91		
SSR-5	14.85	9.65	46.50	29.19	0.48	0.23
SSR-10	15.13	9.38	41.59	28.83	0.72	0.34
SSR-20	15.31	9.27	46.23	27.42	1.26	0.74
SG-0	15.48	11.53	44.85	28.05		
SG-5	15.54	10.70	45.18	27.52	1.44	0.22
SG-10	13.88	9.48	46.70	27.19	1.62	0.23
SG-20	17.60	8.64	45.28	26.60	2.43	0.45

3.1.3 *Electrical resistance analysis*

It is important to measure the electrical resistance based on temperature to determine whether the produced samples show superconducting properties. In this study, the electrical resistance dependence of temperature graphs of the samples produced in $YBa_2Cu_3O_{7-\delta}$ system with two different methods are given in Fig. 5a and b. Electrical resistance measurements were performed by applying ± 5 mA current during 1000 ms to the sample surface by standard four-point contact method. It is seen that the undoped sample produced by SSR method (SSR-0) has higher critical temperature values than the undoped sample produced by SG method (SG-0). In addition, critical temperature value of the samples produced by SSR method are higher than SG method. As an example, T_C^{offset} value of SG-20 is the lowest among all produced sample. Besides, the decrease in the critical temperature value of the samples by the doping ratio, the value of the superconducting transition interval increases (Table 4). It can be

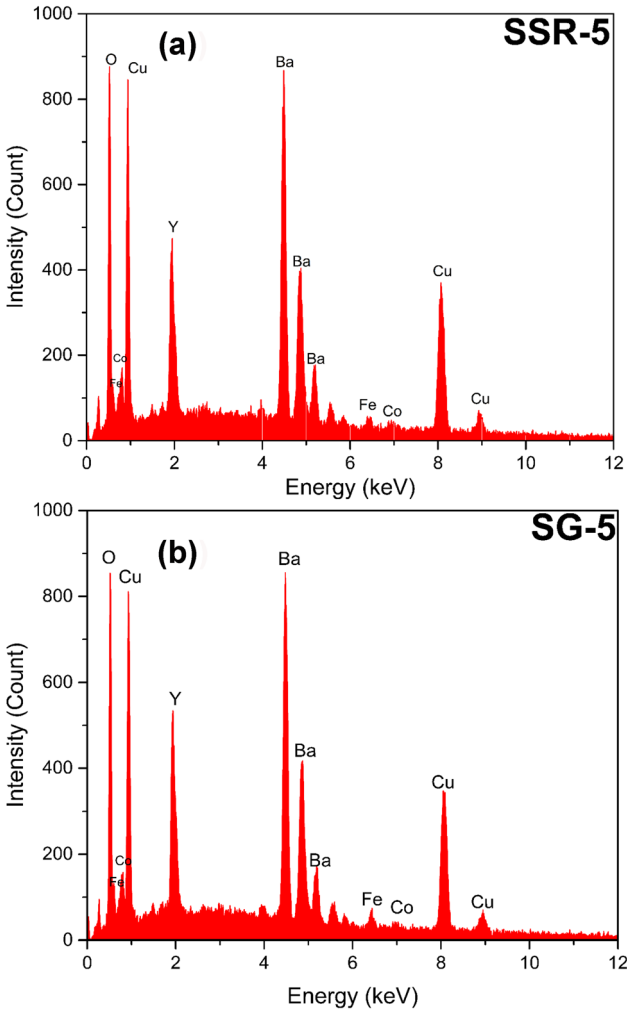

Fig. 4 EDS results of **a** SSR-5, **b** SG-5 superconducting materials

Table 4 Characteristic parameters for produced superconducting samples deduced from temperature-dependent electrical resistance measurements

Sample	Critical Temperature (K)		ΔT_C(K)
	T_C^{onset}	T_C^{offset}	$(T_C^{onset} - T_C^{offset})$
SSR-0	92.96	90.29	2.67
SSR-5	89.54	83.15	6.39
SSR-10	89.26	72.61	16.65
SSR-20	83.97	50.94	33.03
SG-0	92.46	90.00	2.46
SG-5	81.89	73.93	7.96
SG-10	89.08	67.63	21.45
SG-20	65.14	25.31	39.83

interpreted that the some cobalt and iron ions entering the structure affect the electron–phonon coupling [24–26]. As a result, the doping process influenced

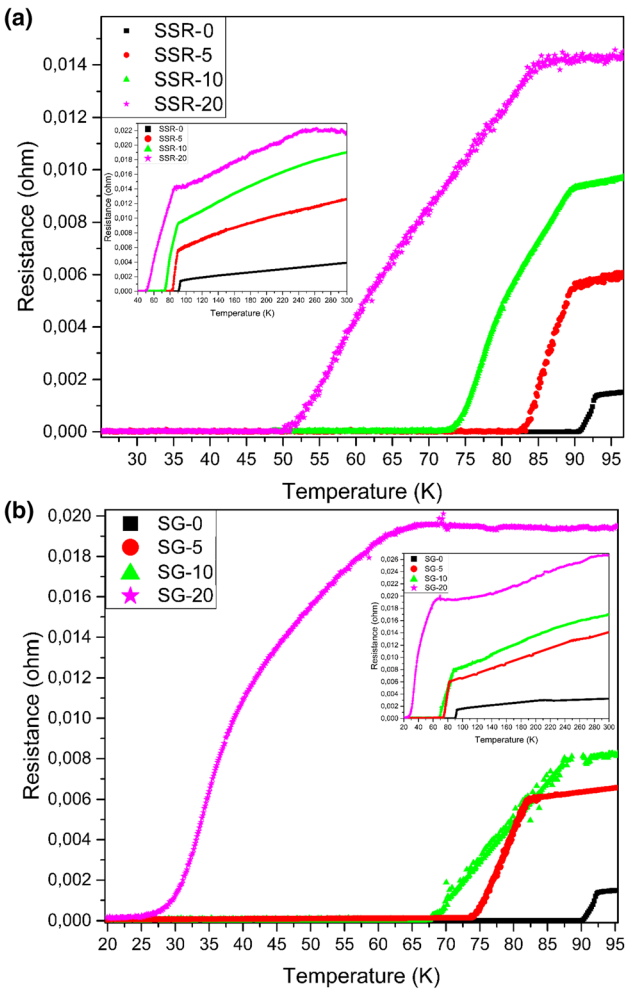

Fig. 5 Temperature-dependent electrical resistance measurements for **a** solid state reaction methods, **b** sol–gel method from 40 to 100 K

the hole concentration in the CuO_2 layer, this cause a decrease in critical transition temperature with the $CoFe_2O$ addition. Table 4 shows that ΔT_C values of SG method are larger when the values are examined. In this case, it is concluded that the doping process is more effective the SG method more than the SSR method. Comparing normal state resistance values, it is seen that the resistance values of the doped samples are at least four times higher than the undoped sample values. It is also interpreted that the increase in the rate of cobalt and iron ions in the structure increases room temperature resistance for both methods. This is expected to be caused by changes in grain boundaries and permanent defects in the structure [27–30].

3.1.4 *Microhardness analysis*

The study and development of the mechanical properties of superconducting samples is very important for the evaluation of their use in industrial materials science and other technological fields [31, 32]. Vicker's microhardness test is one of the most frequently used methods for investigating the microhardness properties of materials, since the damage to the surface is minimal and can be easily applied [33–37]. The sample production method and the response of the sample surface to the applied load are among the factors affecting the microhardness properties. The hardness values of the samples produced in this study were determined by measuring the diagonal lengths obtained by applying five different loads (F = 0.245, 0.490, 0.980, 1.960 and 2.940 N) to the sample surface for 10 s. Mechanical properties were evaluated by calculating microhardness (H_V), elastic modulus (E) and yield strength (Y). Vickers microhardness (H_V) values were calculated using these diagonal lengths by the formula;

$$H_V = 1854.4\left(\frac{F}{d^2}\right) \tag{4}$$

where F is the applied load, $d = \frac{d_1+d_2}{2}$ is the arithmetic mean of the calculated diagonal lengths. Elastic modulus (E) and stress (Y) values were calculated using the following formulas [38];

$$E = 81.9635H_V \tag{5}$$

$$Y \approx H_V/3 \tag{6}$$

The graphs obtained from the Vickers microhardness test and calculated values of H_V, E and Y values for every material at different applied test loads are given in Fig. 6a and b and Table 5, respectively. Above 2 N applied load, no significant change was observed in microhardness values and it is interpreted that the samples reached saturation. SSR-0 and SG-0 samples exhibit RISE (Reverse Indentation Size Effect) behavior which microhardness values increase with increasing applied load. However, as the load applied to the surface of the doped samples increases, the hardness values decreased and this behavior is known as ISE (Indentation Size Effect) [39, 40]. The change in microhardness behavior of samples as a result of doping process; this is predicted to be due to the formation of weak bonding, porosity and impurity phases at the particle

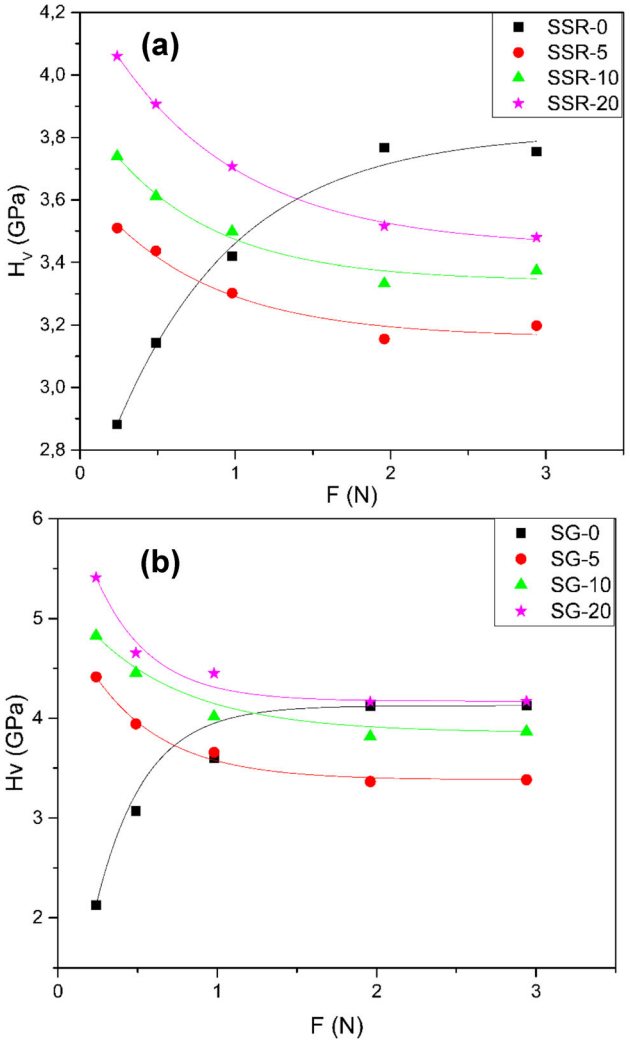

Fig. 6 Variation of Vickers hardness parameters with applied test loads for samples produced by **a** solid state reaction, **b** sol–gel method

boundaries [41, 42]. The microhardness value of the samples produced by the SSR method with the lowest doping rate, although increasing with the doping ratio, did not exceed the microhardness values of the doping sample even at the highest doping rate. Although similar behavior was observed in the samples produced by the SG method, the hardness value of the SG-20 sample with the highest doping ratio was slightly higher than the undoped sample. Comparison of microhardness graphs of samples with same doping ratio are given in Fig. 7a–d. It is clear that all of the samples produced by the SG method have a higher hardness value than the samples produced by the SSR method. As can be seen from Table 5; The SG-20 sample had the highest microhardness, the lowest elastic modulus and the highest tensile strength values, while the SSR-5 sample had the lowest microhardness, the highest elastic modulus and the lowest tensile strength values.

4 Conclusion

In this study, structural, superconducting and mechanical properties of $YBa_2Cu_{3-x}(CoFe_2O_4)xO_{7-\delta}$ copper based superconducting samples produced by solid state reaction and sol–gel methods with x = 0–20% by weight were investigated. As a result of the X-ray analysis, the crystal structures of the samples were determined and lattice parameters were calculated. By comparing the lattice parameters and particle size values calculated for both methods, the samples produced by SSR method were found to be more successful in preserving the orthorhombic structure. Particle boundaries and porosity were examined by SEM analysis. Element distribution of the samples was determined by weight and atomically. It is predicted that cobalt and iron impurities enter the structure with doping and affect the superconducting properties. The critical temperature values obtained by temperature-dependent electrical resistance measurements were examined and it was concluded that the samples produced by SSR method had higher critical temperature values for the same doping ratios. While the critical temperature values decreased due to defects caused by cobalt and iron ions entering the structure and inter-layer compatibility disturbances, ΔT_C values increased. The effects of the addition and the production method on the structure were also observed in microhardness analysis. While both undoped samples exhibited RISE behavior, ISE behavior was observed in doped samples due to factors such as changes in particle boundaries and porosity. The similar relationship between doped samples showed that SSR method could be preferred for softer sample.

Table 5 H_V, E and Y values for every material at different applied test loads

Sample	F (N)	H_V (GPa)	E (GPa)	Y (GPa)	Sample	F (N)	H_V (GPa)	E (GPa)	Y (GPa)
SSR-0	0.245	2.881	236.15	0.960	SG-0	0.245	2.126	174.254	0.709
	0.490	3.143	257.63	1.048		0.490	3.073	251.874	1.024
	0.980	3.420	280.28	1.140		0.980	3.601	295.151	1.200
	1.960	3.768	308.80	1.256		1.960	4.122	337.854	1.374
	2.940	3.755	307.80	1.252		2.940	4.126	338.181	1.375
SSR-5	0.245	3.510	287.712	1.170	SG-5	0.245	4.415	361.883	1.472
	0.490	3.437	281.695	1.146		0.490	3.943	323.204	1.314
	0.980	3.302	270.670	1.101		0.980	3.658	299.799	1.219
	1.960	3.155	258.617	1.052		1.960	3.366	275.896	1.122
	2.940	3.198	262.109	1.066		2.940	3.384	277.343	1.128
SSR-10	0.245	3.740	306.553	1.247	SG-10	0.245	4.829	395.815	1.610
	0.490	3.612	296.083	1.204		0.490	4.456	365.228	1.485
	0.980	3.499	286.788	1.166		0.980	4.017	329.242	1.339
	1.960	3.334	273.228	1.111		1.960	3.817	312.815	1.272
	2.940	3.374	276.515	1.125		2.940	3.867	316.921	1.289
SSR-20	0.245	4.060	332.768	1.353	SG-20	0.245	5.410	443.425	1.803
	0.490	3.907	320.243	1.302		0.490	4.656	381.617	1.552
	0.980	3.707	303.875	1.236		0.980	4.449	364.685	1.483
	1.960	3.516	288.216	1.172		1.960	4.165	341.396	1.388
	2.940	3.480	285.246	1.160		2.940	4.172	341.944	1.391

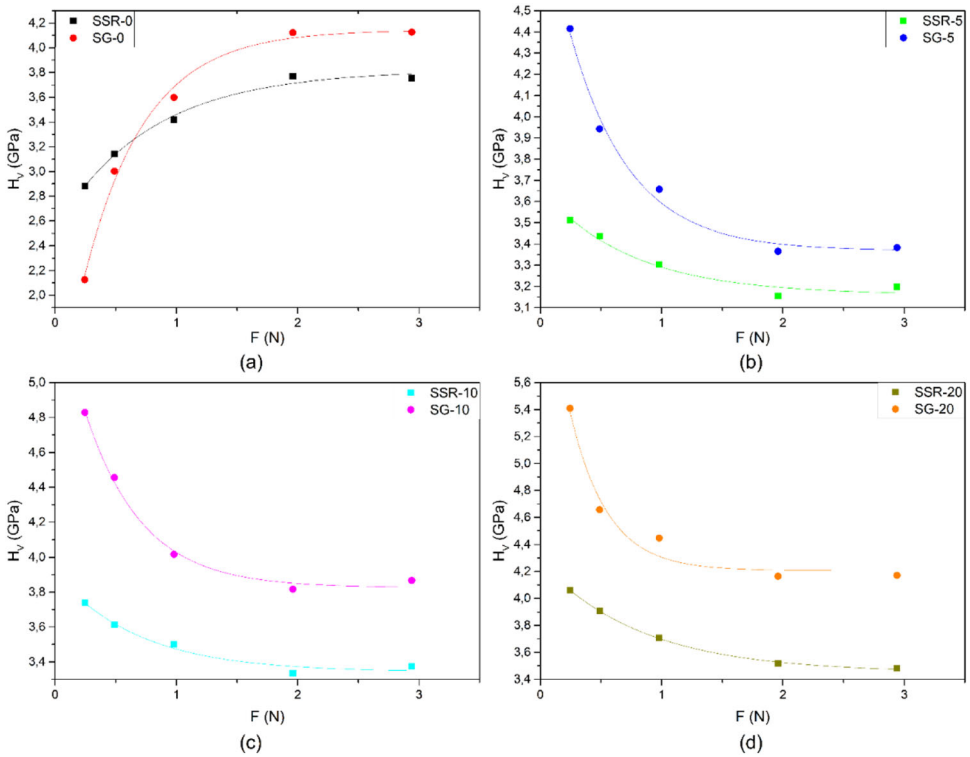

Fig. 7 Comparison chart of samples with same doping ratios produced by different methods; **a** undoped, **b** 0.05, **c** 0.10 and **d** 0.20

References

1. H. Strauven, J.P. Locquet, O.B. Verbeke, Y. Bruynseraede, Oxygen evolution from YBa2Cu3O6.85 high Tc superconductors. Solid State Commun. **65**, 293–6 (1988)
2. E.D. Specht, C.J. Sparks, A.G. Dhere, J. Brynestad, O.B. Cavin, D.M. Kroeger et al., Effect of oxygen pressure on the orthorhombic-tetragonal transition in the high-temperature superconductor YBa2Cu3Ox. Phys Rev B. **37**, 7426–7434 (1988). https://doi.org/10.1103/PhysRevB.37.7426
3. J.D. Jorgensen, B.W. Veal, A.P. Paulikas, L.J. Nowicki, G.W. Crabtree, H. Claus et al., Structural properties of oxygen-deficient YBa2Cu3O7−δ. Phys. Rev. B **41**, 1863–1877 (1990). https://doi.org/10.1103/PhysRevB.41.1863
4. A. Harabor, P. Rotaru, N.A. Harabor, P. Nozar, A. Rotaru, Orthorhombic YBCO-123 ceramic oxide superconductor: structural, resistive and thermal properties. Ceram. Int. **45**(2), 2899–2907 (2019)
5. A. Aliabadi, Y. Akhavan Farshchi, M. Akhavan, A new Y-based HTSC with Tc above 100 K. Physica C **469**, 2012–2014 (2009). https://doi.org/10.1016/j.physc.2009.09.003
6. A. Li, X.N. Ying, Y.B. Qi, X.S. Xu, Z.H. Bao, Q.M. Zhang et al., Effect of zinc doping on the microstructure in YBCO. Physica C **341–348**, 669–670 (2000). https://doi.org/10.1016/S0921-4534(00)00642-0
7. A. Rao, S. Radheshyam, R. Kumar, S. Gupta, C. Meingast, B. Gahtori et al., The influence of Mn doping on the thermal expansion of the high T C superconductor YBa2 (Cu1–x Mn x)3Oy. J. Phys. Condens. Matter **19**, 056208 (2007). https://doi.org/10.1088/0953-8984/19/5/056208
8. S.E. Jasim, M.A. Jusoh, M. Hafiz, R. Jose, Fabrication of superconducting YBCO nanoparticles by electrospinning. Procedia Eng. **148**, 243–248 (2016). https://doi.org/10.1016/j.proeng.2016.06.595
9. Y. Slimani, E. Hannachi, A. Ekicibil, M.A. Almessiere, A.F. Ben, Investigation of the impact of nano-sized wires and particles TiO2 on Y-123 superconductor performance. J. Alloys Compd. **781**, 664–673 (2019). https://doi.org/10.1016/j.jallcom.2018.12.062
10. A. Rao, Influence of Zn doping on the thermal expansion of the high T c superconductor Y1Ba2Cu3Oy. J. Phys. Condens Matter. **16**, 1439–1445 (2004). https://doi.org/10.1088/0953-8984/16/8/024
11. N.P. Liyanawaduge, A. Kumar, R. Jha, B.S.B. Karunarathne, V.P.S. Awana, High field magneto-transport and magnetization study of Y1−xCaxBa2Cu3 (x=0.00–0.25). J. Alloys Compd. **543**, 135–41 (2012)
12. B.A. Malik, K. Asokan, V. Ganesan, D. Singh, M.A. Malik, The magnetoresistance of YBCO/BZO composite superconductors. Physica C **531**, 85–92 (2016). https://doi.org/10.1016/j.physc.2016.11.004
13. B.A. Malik, M.A. Malik, K. Asokan, Magneto transport study of YBCO: Ag composites. Curr. Appl. Phys. **16**, 1270–1276 (2016). https://doi.org/10.1016/j.cap.2016.07.004
14. L.M. Yeoh, M. Ahmad, Characterization and synthesis of Y0.9Ca0.1Ba1.8Sr0.2Cu3O7−δ via combining sol–gel and solid-state route. J. Non Cryst. Solids **354,** 4012–4018 (2008)
15. M. Yilmaz, O. Dogan, Structural and superconducting properties in Y0.6Gd0.4Ba2(Nb)Cu3O7-y cuprates doped with niobium. J Rare Earths. **30**, 241–4 (2012)
16. N.I. Matskevich, T. Wolf, Thermochemical investigation of YBa2Cu3O7−δ superconductor doped by lutetium. J. Alloys Compd. **614**, 415–419 (2014). https://doi.org/10.1016/j.jallcom.2014.06.125
17. A. Baranauskas, D. Jasaitis, A. Kareiva, R. Haberkorn, H. Beck, Sol–gel preparation and characterization of manganese-substituted superconducting YBa2(Cu1−xMnx)4O8 compounds. J. Eur. Ceram. Soc. **21**, 399–408 (2001). https://doi.org/10.1016/S0955-2219(00)00206-5
18. T. Klemkiene, R. Raudonis, A. Beganskiene, A. Zalga, I. Grigoraviciute, A. Kareiva, Scandium and gallium substitution effects in the (Y1−xScx)Ba2Cu4O8 and (Y1−xGax)-Ba2Cu4O8 superconducting oxides. Mater. Chem. Phys. **119**, 208–213 (2010). https://doi.org/10.1016/j.matchemphys.2009.08.059
19. Y. Slimani, E. Hannachi, M.K. Ben Salem, A. Hamrita, A. Varilci, W. Dachraoui et al., Comparative study of nano-sized particles CoFe2O4 effects on superconducting properties of Y-123 and Y-358. Phys. B **450**, 7–15 (2014). https://doi.org/10.1016/j.physb.2014.06.003
20. Y. Slimani, E. Hannachi, M.B. Salem, A. Hamrita, M.B. Salem, F.B. Azzouz, Excess conductivity study in Nano-CoFe2O4-added YBa2Cu3O7−d and Y3Ba5Cu8O18±x superconductors. J. Supercond. Nov. Magn. **28**(10), 3001–10 (2015)
21. Slimani Y, Hannachi E, AF Ben, SM Ben. Comparative Study of the Effect of Magnetic Nanoparticle CoFe2O4 on Fluctuation-Induced Conductivity of Y-123 and Y-358 Superconductors. J Supercond Nov Magn 2019;32:511–519
22. S. Bibekananda, L.R. Krutika, P. Bandana, D. Samal, B. Dhrubananda, Excess conductivity and magnetization of CoFe2O4 combined with $Y_1Ba_2Cu_3O_{7-\delta}$ as a superconductor. J. Phys. Chem. Solids **132**, 187 (2019). https://doi.org/10.1016/j.jpcs.2019.04.035
23. U. Schwingenschlögl, C. Schuster, Quantitative calculations of charge-carrier densities in the depletion layers at YBa2-Cu3O7−δ interfaces. Phys. Rev. B **79**, 092505 (2009). https://doi.org/10.1103/PhysRevB.79.092505

24. Y. Zalaoglu, F. Karaboga, C. Terzioglu, G. Yildirim, Improvement of mechanical performances and characteristics of bulk Bi-2212 materials exposed to Au diffusion and stabilization of durable tetragonal phase by Au. Ceram Int. **43**, 6836–6844 (2017). https://doi.org/10.1016/j.ceramint.2017.02.104
25. P.B. Allen, W.E. Pickett, H. Krakauer, Anisotropic normal-state transport properties predicted and analyzed for high- Tc oxide superconductors. Phys. Rev. B. **37**, 7482–7490 (1988). https://doi.org/10.1103/PhysRevB.37.7482
26. N.K. Saritekin, M. Pakdil, G. Yildirim, M. Oz, T. Turgay, Decrement in metastability with Zr nanoparticles inserted in Bi-2223 superconducting system and working principle of hybridization mechanism. J. Mater. Sci. Mater. Electron. **27**, 956–965 (2016). https://doi.org/10.1007/s10854-015-3839-9
27. S. Martin, M. Gurvitch, C.E. Rice, A.F. Hebard, P.L. Gammel, R.M. Fleming et al., Nonlinear temperature dependence of the normal-state resistivity in YBa2Cu4O8±δ films. Phys. Rev. B **39**, 9611–9613 (1989). https://doi.org/10.1103/PhysRevB.39.9611
28. R. Shabna, P.M. Sarun, S. Vinu, U. Syamaprasad, Charge carrier localization and metal to insulator transition in cerium substituted (Bi, Pb)-2212 superconductor. J. Alloys Compd. **493**, 11–16 (2010). https://doi.org/10.1016/j.jallcom.2009.12.047
29. D.M. Newns, P.C. Pattnaik, C.C. Tsuei, Role of Van Hove singularity in high-temperature superconductors: mean field. Phys. Rev. B. **43**, 3075–3084 (1991). https://doi.org/10.1103/PhysRevB.43.3075
30. Y. Zalaoglu, G. Yildirim, C. Terzioglu, Magnetoresistivity study on Cr added Bi-2212 superconductor ceramics with experimental and theoretical approaches. J. Mater. Sci. Mater. Electron. **24**, 239–247 (2013). https://doi.org/10.1007/s10854-012-0723-8
31. Miao H, Meinesz M, Czabaj B, Parrell J, Hong S, Balachandran U (Balu), et al. Microstructure and Jc improvements in multifilamentary Bi-2212/Ag wires for high field magnet applications. AIP Conf. Proc., vol. 986, AIP; 2008, p. 423–30. https://doi.org/10.1063/1.2900377.
32. H.H. Xu, L. Cheng, S.B. Yan, D.J. Yu, L.S. Guo, X. Yao, Recycling failed bulk YBCO superconductors using the NdBCO/YBCO/MgO film-seeded top-seeded melt growth method. J. Appl. Phys. **111**, 103910 (2012). https://doi.org/10.1063/1.4720400
33. Awad R, Abou-Aly AI, Abdel Gawad MMH, G-Eldeen I, The influence of SnO2 nano-particles addition on the Vickers microhardness of (Bi, Pb)-2223 superconducting phase. J. Supercond. Nov. Magn. **25**, 739–745 (2012)
34. Y. Yoshino, A. Iwabuchi, K. Noto, N. Sakai, M. Murakami, Vickers hardness properties of YBCO bulk superconductor at cryogenic temperatures. Physica C **357–360**, 796–798 (2001). https://doi.org/10.1016/S0921-4534(01)00367-7
35. U. Kölemen, S. Çelebi, Y. Yoshino, A. Öztürk, Mechanical properties of YBCO and YBCO+ZnO polycrystalline superconductors using Vickers hardness test at cryogenic temperatures. Physica C **406**, 20–26 (2004). https://doi.org/10.1016/j.physc.2004.02.174
36. Srour A, Malaeb W, Rekaby Mand Awad R, Mechanical properties of the $(BaSnO_3)_x/Cu_{0.5}Tl_{0.5}Ba_2Ca_2Cu_3O_{10-\delta}$ superconductor phase. Phys. Scr. **92,** 104002 (2017)
37. K. Habanjar, A. Najem, A.M. Abdel-Gaber, R. Awad, Effect of pelletization pressure on the physical and mechanical properties of (Bi, Pb)-2223 superconductors. Phys. Scr. (2020). https://doi.org/10.1088/1402-4896/ab7f46
38. Asikuzun E, Ozturk O, Cetinkara HA, Yildirim G, Varilci A, Y\ilmazlar M, et al. Vickers hardness measurements and some physical properties of Pr2O3 doped Bi-2212 superconductors. J Mater Sci Mater Electron. 2012;23:1001–10. doi:https://doi.org/10.1007/s10854-011-0537-0.
39. R. Awad, A.I. Abou Aly, M. Kamal, M. Anas, Mechanical properties of (Cu0.5TI0.5)-1223 substituted by Pr. J Supercond Nov Magn. **24**, 1947–56 (2011)
40. K. Sangwal, On the reverse indentation size effect and microhardness measurement of solids. Mater. Chem. Phys. **63**, 145–152 (2000). https://doi.org/10.1016/S0254-0584(99)00216-3
41. M. Dogruer, O. Gorur, F. Karaboga, G. Yildirim, C. Terzioglu, Zr diffusion coefficient and activation energy calculations based on EDXRF measurement and evaluation of mechanical characteristics of YBa2Cu3O7−x bulk superconducting ceramics diffused with Zr nanoparticles. Powder Technol. **246**, 553–560 (2013). https://doi.org/10.1016/j.powtec.2013.06.018
42. M. Dogruer, C. Terzioglu, G. Yildirim, O. Gorur, Significant change in mechanical properties of YBa2Cu3O7−xBulk superconductors diffused with Sn nanoparticles. J. Supercond. Nov. Magn. **27**, 755–761 (2014). https://doi.org/10.1007/s10948-013-2379-x